International Journal of Science and Engineering Applications
Volume 7–Issue 06,85-93, 2018, ISSN:-2319–7560

Investigation of Ride Quality of the Truck Using Sinusoidal Road Pavement in Low and High Speed by Utilizing Lagrange Method

Ali Rahmani
Assistant Professor,
Department of Mechanical and Materials Engineering
Shahid Rajaee Teacher Training University,
Tehran, Iran

Pedram Hoseini
MSc Student
Department of Mechanical Engineering
Amirkabir University of Technology
Tehran, Iran

Abstract: In this research, ride quality of a truck is investigated to understand vibration specifications of the multi-degree of freedom 3-axle rigid truck. for this purpose, a Benz 2624 model have been modelled. An off-road duty is considered for this analysis. A modeling procedure and simulation of the truck is produced in this research. The system is modelled by a linear model which contains the seat and cab suspensions, rigid live axles, and also suspension geometries, the motion equations and system matrices are obtained by utilizing the Lagrange's equation. Then, a numerical central difference method is utilized to gain the system responses subject to the sinusoidal road excitations. Truck's physical parameters and dynamic properties of its components are not well-known therefore these properties have been achieved by modeling the truck in SOLIDWORKS software. Finally, a code based on these equations is developed in MATLAB software to calculate system time responses under different cases, which contains low and high drive frequency of the truck. The developed model can also be used for newer trucks with some modifications to change the current model it's necessary to have accurate information for input data.

Keywords: Multi-axles truck, Lagrange equations, Road excitations, Vibration analysis, System response

1. INTRODUCTION

Modeling procedure is an important part in engineering. The two types of the modeling are: Numerical and physical modeling, which used widely in engineering [1-12]. Vibration modeling is one of the applications for modeling and analyzing in engineering. For example, Vibration has an important role in design and maintenance of bridge structures especially when the frequency is close to bridge's natural vibrations [13-14]. Many fields and products like, e.g., aerospace [15-19], automobile, transportation, satellite with high frequency switches, electric vehicle, buildings, and so on have been improved by the contribution of vibration analysis [20]. Identification and suppression of unwanted vibrations are the most common goal to improve product quality. As a real-world example, Multi-axel truck need this procedure to breakdown its vibrations.

Dynamic excitation causes by the interaction between vehicle's wheels and road surface. Different vibration levels occur by the amount of elevation of the road surface unevenness and the vehicle's speed [21-22]. Heavy vehicles produce the most perceptible vibrations. A vehicle model is used to describe the dynamic behavior of the vehicle, which is consisted of discrete masses, springs, friction elements and dampers [23-27]. By obtaining a linear model of a vehicle with high output and acceptable efficiency, the calculation of axle loads is facilitated by using Frequency Response Functions [28]. Local road unevenness is expressed by utilizing deterministic function, which is showing the deviation of the travelled surface from a true planar surface. By the utilizing a Power Spectral Density the global road unevenness can also be defined in a stochastic way [29-35].

Many models such as quarter, bicycle, half and full models of vehicle have been investigated with different numbers of DoF for vehicle dynamics [36-41]. One of the most famous models for vehicles is Eight-DoF model, including forward, lateral, yaw and roll motion and four DoF for travel of each wheel [30]. In the literature, multibody system dynamic models of vehicles have also been proposed. For instance, Rahmani Hanzaki et al. proposed a methodology for dynamic analysis of a multibody system with spherical joints. As an example, for that they have considered a suspension system of a vehicle [31]. Applying this methodology to a three-axle truck makes complicated computation. Therefore, other discrete model for the truck has been employed. For example, Tabatabaee developed a 16-DoF non-linear model an articulated vehicle, which is validated experimentally [32].

In this paper a survey on the equations of motion will be presented, by the use of Lagrange equation, to finally determine system responses of a complete 3-D rigid three-axle truck model subject to sinusoidal road excitations, in different cases and different speeds. This analysis can be useful to better understand the coupled motions of the truck's wheels. The validation of equations has been verified by utilizing ADAMS software in our previous paper [33-35]. The developed 19 DoF model can be used for other trucks by applying changes in material properties and adding estimations. Mathematical modeling that was discussed in Zeidi et al. [36-41] is continued in the present study for discretization of 19 DOF truck. Impact of CO emission, which was discussed in Aghaei et al. [42], has also been used in the current model as input for the current model.

2. MODELING THE TRUCK

Experimental methods are the most reasonable techniques to acquire mass properties of components of a manufactured vehicle, but these techniques are very costly. Therefore, for this work, to obtain masses, centers of mass, moments of inertia etc. of the three-axle truck a SOLIDWORKS model of the vehicle have been modeled and utilized. For dynamic simulation of the truck these physical properties are highly

necessary. Figures 1 and 2 shows two views of the assembled truck model, and some of the trucks components are depicted, respectively. In modelling this truck, the weighty components are modeled precisely, such as chassis, cabin, differentials, tires, springs etc. Non-homogeneous material is assigned to this model since differential consists of several material and precision of properties, which are acquired from this model are more acceptable.

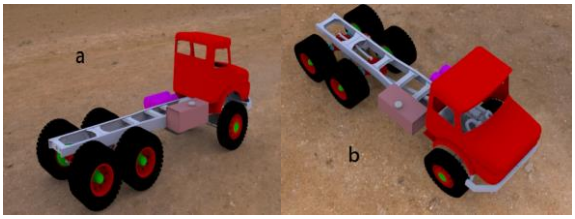

Figure 1. CAD model of the three-axle truck

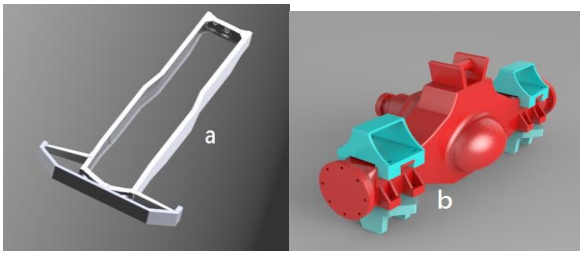

Figure 2. Two main CAD modelled components of the truck; a) chassis, b) axle with differential

2.1 Governing the Equations

The Lagrange method is utilized to obtain dynamic behavior of the mentioned three-axle truck. 19-DoF mathematical model is considered for the truck. M1, M2 and M3 are the axles of the truck as shown in Figure 3. Blue springs are considered on behalf of tires and red springs as leaf springs of the suspensions systems. Green springs are counted for connecting cabin to the frame and finally, purple spring is used to suspend driver's seat with respect to the cabin. As the rests, W, θ, and φ illustrate displacement, roll, and pitch of the truck in this dynamic analysis. Hence, the 19 DoFs are as follow:

- Driver seat bounce, one degree; w_106;
- Cab bounce, pitch and roll, three degrees; orderly w_104, θ_104, φ_104;
- Chassis bounce (sprung mass), pitch and roll, three degrees; w_100, φ_100, θ_100, respectively:
- Front axle, its bounce and roll, two degrees; orderly w_101, θ_101;
- Intermediate axle, bounce and roll, two degrees; orderly w_102 , θ_102;
- Rear axle, bounce and roll, two degrees; orderly w_103, θ_103;
- 6 bounce motion of the 6 wheels; w_1, w_2, w_3, w_4, w_5, w_6; where w_1 and ; w_2are the bounce of left and right steer wheels, respectively; w_3 and w_4 are the bounce of left and right wheels of the middle axle, correspondingly; w_5 and w_6are the bounce of left and right wheels of rear axle, respectively.

The vector of coordinates for the vehicle is written as:

W_19=[w_106 w_104 θ_104 φ_104 〖w〗_(100 θ_100) φ_100 w_101 θ_101 w_102 θ_102 w_103 θ_103 w_1 w_2 w_3 w_4 w_5 w_6]^T

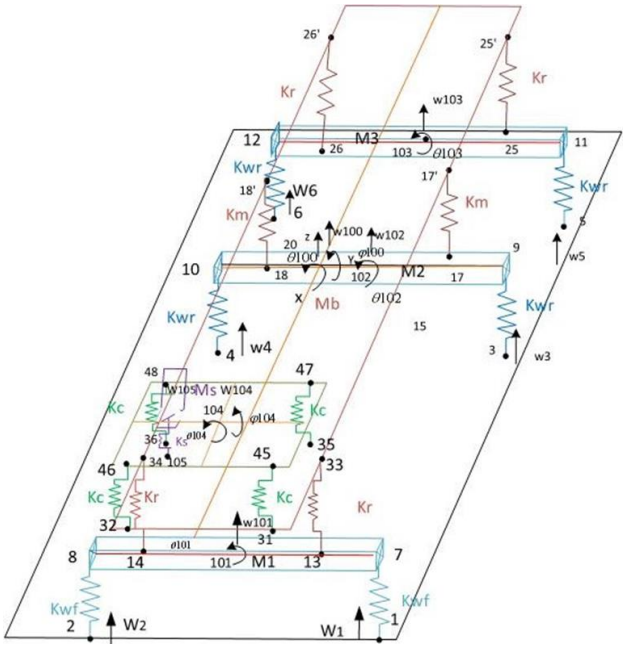

Figure 3. The scheme of the 19-DoF model for the truck

Figure 4(a) shows truck model in X-Z plane and distances between different important points. In addition, Figure 4(b) indicates the model in Y-Z plane and the related parameters.

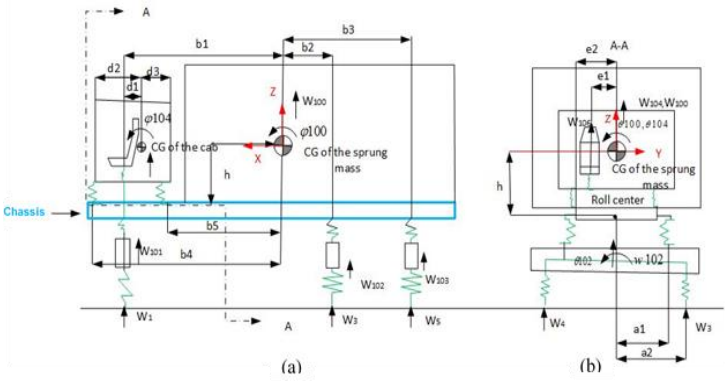

Figure 4. CGs (Center of gravity) and other essential parameters of the truck.

2.2 Motion Equations

The well-known Lagrange equation for this system is in the following form:

$$\frac{d}{dt}\left(\frac{dT}{d\dot{W}_{19}}\right)-\left(\frac{dT}{dW_{19}}\right)+\left(\frac{dP}{dW_{19}}\right)+\left(\frac{dR}{d\dot{W}_{19}}\right)=0 \qquad (2)$$

Where T, P and R are the kinematic, potential and dissipation energies of the system, respectively.

The kinetic energy part of the system is obtained as:

$$\begin{aligned}T=&\tfrac{1}{2}M_s(\dot{W}106)^2+\tfrac{1}{2}M_c(\dot{W}104)^2+\\&\tfrac{1}{2}M_b(\dot{W}100)^2+\tfrac{1}{2}M_1(\dot{W}101)^2+\tfrac{1}{2}M_2(\dot{W}102)^2+\\&\tfrac{1}{2}M_3(\dot{W}103)^2+\tfrac{1}{2}I_{cx}(\dot{\theta}104)^2+\tfrac{1}{2}I_{bx}(\dot{\theta}100)^2+\\&\tfrac{1}{2}I_{1x}(\dot{\theta}101)^2+\tfrac{1}{2}I_{2x}(\dot{\theta}102)^2+\tfrac{1}{2}I_{3x}(\dot{\theta}103)^2+\\&\tfrac{1}{2}I_{cy}(\dot{\theta}104)^2+\tfrac{1}{2}I_{by}(\dot{\theta}100)^2\end{aligned} \qquad (3)$$

Moreover, the potential energy part of the system is as follow:

$$\begin{aligned}P=&\tfrac{1}{2}K_s(W106-W105)^2+\tfrac{1}{2}K_c(W45-W31)^2+\\&\tfrac{1}{2}K_c(W46-W32)^2+\tfrac{1}{2}K_c(W47-W35)^2+\\&\tfrac{1}{2}K_c(W48-W36)^2+\tfrac{1}{2}K_f(W33-W13)^2+\\&\tfrac{1}{2}K_f(W34-W14)^2+\tfrac{1}{2}K_m(W17`-W17)^2+\\&\tfrac{1}{2}K_m(W18`-W18)^2+\tfrac{1}{2}K_r(W25`-W25)^2+\\&\tfrac{1}{2}K_r(W26`-W26)^2+\tfrac{1}{2}K_{Wf}(W7-W1)^2+\\&\tfrac{1}{2}K_{Wf}(W8-W2)^2+\tfrac{1}{2}K_{Wr}(W9-W3)^2+\\&\tfrac{1}{2}K_{Wr}(W10-W4)^2+\tfrac{1}{2}K_{Wr}(W11-W5)^2+\\&\tfrac{1}{2}K_{Wr}(W12-W6)^2\end{aligned} \qquad (4)$$

And the dissipation energy part of the system is:

$$\begin{aligned}R=&\tfrac{1}{2}c_s(\dot{W}106-\dot{W}105)^2+\tfrac{1}{2}c_{c1}(\dot{W}45-\\&\dot{W}31)^2+\tfrac{1}{2}c_{c2}(\dot{W}46-\dot{W}32)^2+\tfrac{1}{2}c_{c3}(\dot{W}47-\\&\dot{W}35)^2+\tfrac{1}{2}c_{c4}(\dot{W}48-\dot{W}36)^2+\tfrac{1}{2}c_1(\dot{W}33-\dot{W}13)^2+\\&\tfrac{1}{2}c_2(\dot{W}34-\dot{W}14)^2+\tfrac{1}{2}c_{s3}(\dot{W}17`-\dot{W}17)^2+\\&\tfrac{1}{2}c_{s4}(\dot{W}18`-\dot{W}18)^2+\tfrac{1}{2}c_{s5}(\dot{W}25`-\dot{W}25)^2+\\&\tfrac{1}{2}c_{s6}(\dot{W}26`-\dot{W}26)^2\end{aligned} \qquad (5)$$

The equations of motion can be organized by differentiating of T, P and R with respect to the coordinates and time according to eq. (2), this gives:

$$M.\ddot{W}+C.\dot{W}+K.W=0 \qquad (6)$$

In which M_{19}, K_{19} and C_{19} are mass matrix, stiffness matrix and damping matrix of the 19 DoF of the truck-poster system model, respectively. In this equation, $\ddot{W}_{19}$, $\dot{W}_{19}$ and W_{19} are acceleration vector, velocity vector and displacement vector of the 19 DoF truck model. In addition, the diagonal system mass matrix, M_{19}, is calculated as follow:

$$M_{19}=\mathrm{diag}[M_s\ M_c\ I_{cx}\ I_{cy}\ M_b\ I_{bx}\ I_{by}\ M_1\ I_{1x}\ M_2\ I_{2x}\ M_3\ I_{3x}\ M_{01}\ M_{02}\ M_{03}\ M_{04}\ M_{05}\ M_{06}]$$

Where, "diag" illustrates that the M_{19} matrix is diagonal; M_s to M_{06} are located on the main diagonal of this matrix. In this relation, M_s and M_c are masses of the seat and the driver, and the cab, respectively; I_{cx} and I_{cy} are inertia of the cab about X and Y axes, correspondingly. In the following, M_b, I_{bx}, and I_{by} point to sprung mass, inertia of the sprung mass about X and Y axes, respectively; Also, 1, 2, and 3 as the indexes in order point to the front axle, middle axle, and the rear axle of the truck. Similarly, M_{01} to M_{06} shows the masses of the front left to rear right wheels, as well. The 19 nonzero values have been achieved from the truck model in Solidworks software by utilizing mass properties. Now, the system damping matrix and stiffness matrix can be written in the following form:

$$C_{19}=\begin{bmatrix}C_{1,1}&C_{1,2}&\cdots&C_{1,19}\\C_{2,1}&C_{2,2}&&C_{2,19}\\\vdots&&\ddots&\vdots\\C_{19,1}&C_{19,2}&\cdots&C/_{19,19}\end{bmatrix},\qquad K_{19}=\begin{bmatrix}K_{1,1}&K_{1,2}&\cdots&K_{1,19}\\K_{2,1}&K_{2,2}&&K_{2,19}\\\vdots&&\ddots&\vdots\\K_{19,1}&K_{19,2}&\cdots&K_{19,19}\end{bmatrix}$$

The non-zero components of C_{19} and K_{19} are as following:

$$\begin{aligned}&C_{1,1}=C_s,\ C_{1,2}=C_{2,1}=-C_s,\ C_{1,3}=C_{3,1}=C_s.e_1,\\&C_{1,4}=C_{4,1}=C_s.d_1\\&C_{2,2}=C_s+C_{c1}+C_{c2}+C_{c3}+C_{c4},\\&C_{2,3}=C_{3,2}=-C_s.e_1+C_{c1}.e_2-C_{c2}.e_2+C_{c3}.e_2-\\&C_{c4}.e_2\\&C_{2,4}=C_{4,2}=-C_s.d_1-C_{c1}.d_2-C_4.C_2.d_2+C_{c3}.d_3+\\&C_{c4}.d_3\\&C_{2,5}=C_{5,2}=-C_{c1}-C_{c2}-C_{c3}-C_{c4},\\&C_{2,6}=C_{6,2}=C_{3,5}=C_{5,3}=-C_{c1}.e_2+C_{c2}.e_2-\\&C_{c3}.e_2+C_{c4}.e_2\\&C_{2,7}=C_{7,2}=C_{c1}.b_4+C_{c2}.b_4+C_{c3}.b_5+C_{c4}.b_5;\\&C_{3,3}=C_s.e_1^2+C_{c1}.e_2^2+C_{c2}.e_2^2+C_{c3}.e_2^2+C_{c4}.e_2^2,\\&C_{3,4}=C_{4,3}=C_s.d_1.e_1-C_{c1}.d_2.e_2+C_{c2}.d_2.e_2+\\&C_{c3}.d_3.e_2-C_{c4}.d_3.e_2\\&C_{3,6}=C_{6,3}=-C_{c1}.e_2^2-C_{c2}.e_2^2-C_{c3}.e_2^2-C_{c4}.e_2^2,\\&C_{3,7}=C_{7,3}=C_{c1}.b_4.e_2-C_{c2}.b_4.e_2+C_{c3}.b_5.e_2-\\&C_{c4}.b_5.e_2\end{aligned}$$

$C_{4,4} = C_s.d_1^2 + C_{c1}.d_2^2 + C_{c2}.d_2^2 + C_{c3}.d_3^2 + C_{c4}.d_3^2,$
$C_{4,5} = C_{5,4} = C_{c1}.d_2 + C_{c2}d_2 - C_{c3}.d_3 - C_{c4}.d_3,$

$C_{4,6} = C_{6,4} = C_{c1}.d_2.e_2 - C_{c2}.d_2.e_2 - C_{c3}.d_3.e_2 + C_{c4}.d_3.e_2$
$C_{4,7} = C_{7,4} = -C_{c1}.b_4.d_2 - C_{c2}.b_4.d_2 + C_{c3}.b_5.d_3 + C_{c4}.b_5.d_3;$

$C_{5,5} = C_{c1} + C_{c2} + C_{c3} + C_{c4} + C_1 + C_2 + C_3.l_2^2/l_1 + C_4.l_2^2/l_1 + C_5.l_2^2/l_1 + C_6.l_2^2/l_1,$
$C_{5,6} = C_{6,5} = C_{c1}.e_2 - C_{c2}.e_2 + C_{c3}.e_2 - C_{c4}.e_2 + C_1.a_1 - C_2.a_1 + C_3.l_2^2/l_1.a_1 - C_4.l_2^2/l_1.a_1 + C_5.l_2^2/l_1.a_1 - C_6.l_2^2/l_1.a_1;$
$C_{5,7} = C_{7,5} = -C_{c1}.b_4 - C_{c2}.b_4 - C_{c3}.b_5 - C_1.b_1 - C_2.b_1 + C_3.l_2^2/l_1.b_2 + C_4.l_2^2/l_1.b_2;$
$C_{5,8} = C_{8,5} = -C_1 - C_2,$
$C_{5,9} = C_{9,5} = C_{6,8} = C_{8,6} = -C_1.a_1 + C_2.a_1,$
$C_{5,10} = C_{10,5} = -C_3.l_2^2/l_1 - C_4.l_2^2/l_1;$

$C_{5,11} = C_{11,5} = C_{6,10} = C_{10,6} = -C_3.l_2^2/l_1.a_1 + C_4.l_2^2/l_1.a_1$
$C_{5,12} = C_{12,5} = C_{6,12} = C_{12,6} = -C_5.l_2^2/l_1 + C_6.l_2^2/l_1;$

$C_{5,13} = C_{13,5} = -C_5.l_2^2/l_1.a_1 + C_6.l_2^2/l_1.a_1,$
$C_{6,6} = C_{c1}.e_2^2 + C_{c2}.e_2^2 + C_{c3}.e_2^2 + C_{c4}.e_2^2 + C_1.a_1^2 + C_2.a_1^2 + C_3.l_2^2/l_1.a_1^2 + C_4.l_2^2/l_1.a_1^2 + C_5.l_2^2/l_1.a_1^2 + C_6.l_2^2/l_1.a_1^2;$
$C_{6,7} = C_{7,6} = -C_{c1}.b_4.e_2 + C_{c2}.b_4.e_2 - C_{c3}.b_5.e_2 + C_{c4}.b_5.e_2 - C_1.a_1.b_1 + C_2.a_1.b_1 + C_3.l_2^2/l_1.b_2.a_1 - C_4.l_2^2/l_1.b_2.a_1 + C_5.l_2^2/l_1.a_1 - C_6.l_2^2/l_1.a_1;$

$C_{6,9} = C_{9,6} = -C_1.a_1^2 - C_2.a_1^2,$
$C_{6,11} = C_{11,6} = -C_3.l_2^2/l_1.a_1^2 - C_4.l_2^2/l_1.a_1^2,$
$C_{6,13} = C_{13,6} = -C_5.l_2^2/l_1.a_1^2 - C_6.l_2^2/l_1.a_1^2,$

$C_{7,7} = C_{c1}.b_4^2 + C_{c2}.b_4^2 + C_{c3}.b_5^2 + C_{c4}.b_5^2 + C_1.b_1^2 + C_2.b_1^2 + C_3.l_2^2/l_1.b_2^2 + C_4.l_2^2/l_1.b_2^2 + C_5.l_2^2/l_1.b_3^2 + C_6.l_2^2/l_1.b_3^2;$

$C_{7,8} = C_{8,7} = C_1.b_1 + C_2.b_1,$
$C_{7,9} = C_{9,7} = C_1.a_1.b_1 - C_2.a_1.b_1,$
$C_{7,10} = C_{10,7} = -C_3.l_2^2/l_1.b_2 - C_4.l_2^2/l_1.b_2,$

$C_{7,11} = C_{11,7} = -C_3.l_2^2/l_1.b_2.a_1 + C_4.l_2^2/l_1.b_2.a_1,$
$C_{7,12} = C_{12,7} = -C_5.l_2^2/l_1.b_3 - C_6.l_2^2/l_1.b_3,$

$C_{7,13} = C_{13,7} = -C_5.l_2^2/l_1.b_3.a_1 + C_6.l_2^2/l_1.b_3.a_1,$
$C_{8,8} = C_1 + C_2, C_{8,9} = C_{9,8} = C_1.a_1 - C_2.a_1;$

$C_{9,9} = C_{9,8} = C_1.a_1^2 + C_2.a_1^2,$
$C_{10,10} = C_3.l_2^2/l_1 + C_4.l_2^2/l_1, C_{10,11} = C_{11,10} = C_3.l_2^2/l_1.a_1 - C_4.l_2^2/l_1.a_1;$
$C_{11,11} = C_3.l_2^2/l_1.a_1^2 + C_4.l_2^2/l_1.a_1^2,$
$C_{12,12} = C_5.l_2^2/l_1 + C_6.l_2^2/l_1,$
$C_{12,13} = C_{13,12} = C_5.l_2^2/l_1.a_1 - C_6.l_2^2/l_1.a_1$

$C_{13,13} = C_5.l_2^2/l_1.a_1^2 + C_6.l_2^2/l_1.a_1^2;$

$K_{1,1} = K_s,\ K_{1,2} = -K_s,\ K_{1,3} = K_s.e_1,\ K_{1,4} = K_s.d_1;$

$K_{2,1} = -K_s, K_{2,2} = 4K_c + K_s, K_{2,3} = -K_s.e_1,$
$K_{2,4} = K_c(2d_3 - 2d_2) - K_s.d_1, K_{2,5} = -4K_c, ,$
$K_{2,7} = K_c(2b_5 + 2b_4);$

$K_{3,1} = K_s.e_1,\ K_{3,2} = -K_s.e_1,$
$K_{3,3} = 4K_c.e_2^2 + K_s.e_1^2,\ K_{3,4} = K_s.e_1.d_1;$

$K_{4,1} = K_s.d_1, K_{4,2} = -K_s.d_1 - 2K_c.d_2 + 2K_{c3}.d_3,$
$K_{4,3} = K_s.d_1.e_1, K_{4,4} = K_s.d_1^2 + 2K_c(d_2^2 + d_3^2),$
$K_{4,5} = 2K_c(d_2 - d_3), K_{4,6} = -2K_c.d_3.e_2,$
$K_{4,7} = -2K_c.d_2.b_4 + 2K_c.d_3.b_5;$

$K_{5,2} = -4K_c, K_{5,4} = -2K_c.d_3$
$K_{5,5} = 2K_f + 2K_m + 2K_r + 4K_c,$
$K_{5,6} = 2(K_f + K_m + K_r).a_1 + 2K_c.e_2,$
$K_{5,7} = -2K_f.b_1 + 2K_m.b_2 + 2K_r.b_3 - 2K_c.b_4,$
$K_{5,8} = -2K_f, , K_{5,10} = -2K_m, K_{5,11} = 2K_m.a_1$
$K_{5,12} = -2K_r;$

$K_{6,2} = -2K_c.e_2,\ K_{6,3} = -2K_c.e_2^2,$
$K_{6,4} = -2K_c.e_2.d_3,$
$K_{6,5} = 2(K_f + K_m + K_r).a_1 + 2K_c.e_2,$
$K_{6,6} = 2(K_f + K_m + K_r).a_1^2 + 4K_c.e_2^2,$
$K_{6,7} = -2K_f.a_1.b_1 - 2K_m.a_1.b_2 + 2K_r.a_1.b_3 - 2K_c.e_2.b_4$
$, K_{6,8} = -2K_f.a_1, , K_{6,12} = -2K_r.a_1;$

$K_{7,2} = 4K_c.b_4, K_{7,4} = -2K_c.b_4.d_2 + 2K_c.b_5.d_3,$
$K_{7,5} = -2K_f.b_1 + 2K_m.b_2 + 2K_r.b_2 - 2K_c.b_4 - 2K_c.b_5$
$K_{7,6} = -2K_f.a_1.b_1 + 2K_5.a_1.b_3 + 2K_c.e_2.b_4,$
$K_{7,7} = 2K_f.b_1^2 + 2K_m.b_2^2 + 2K_r.b_3^2 + 2K_c.b_4^2 + 3K_c.b_5^2$
$, K_{7,8} = 2K_f.b_1, K_{7,10} = -2K_m.b_2,$
$K_{7,11} = 2K_m.b_2.a_1, K_{7,12} = -2K_r.b_3;$

$K_{8,6} = -2K_f.a_1, K_{8,7} = 2K_f.b_1, K_{8,8} = 2K_f + 2K_{wf};$

$K_{9,9} = 2K_{wf}.a_2{}^2 + 2K_1.a_1{}^2\, K_{9,14} = -K_{wf}.a_2,$
$K_{9,15} = K_{wf}.a_2;$

$K_{10,5} = -2K_m, K_{10,6} = -2K_m.a_1, K_{10,7} = -2K_3.b_2.,$
$K_{10,10} = 2K_{wr}, K_{10,11} = -2K_3.a_1, K_{10,16} = -K_{wr},$
$K_{10,17} = -K_{wr};$

$K_{11,5} = 2K_m.a_1, K_{11,7} = 2K_m.b_2.a_1,$
$K_{11,10} = -2K_m.a_1, K_{11,11} = 2K_m.a_1{}^2 + 2K_{wr}.a_2{}^2,$
$K_{11,16} = -K_{wr}.a_2, K_{11,17} = K_{wr}.a_2;$

$K_{12,5} = -2K_r, K_{12,6} = -2K_5.a_1, K_{12,7} = -2K_r.b_3,$
$K_{12,12} = 2K_{wr}, , K_{12,18} = -2K_{wr};$

$K_{13,13} = 2K_{wr}.a_2{}^2 + 2K_5.a_1{}^2, K_{13,18} = -K_{wr}.a_2,$
$K_{13,19} = -K_{wr}.a_2;$

$K_{14,8} = -K_{wf}, K_{14,9} = -K_{wf}.a_2, K_{14,14} = K_{wf};$

$K_{15,8} = -K_{wf}, K_{15,9} = K_{wf}.a_2, K_{15,15} = K_{wf};$

$K_{16,10} = -K_{wr}, K_{16,11} = -K_{wr}.a_2, K_{16,16} = K_{wr};$

$K_{17,10} = -K_{wr}, K_{17,11} = K_{wr}.a_2, K_{17,17} = K_{wr};$

$K_{18,12} = -K_{wr}, K_{18,13} = K_{wr}.a_2, K_{18,18} = K_{wr};$

$K_{19,12} = -K_{wr}, K_{19,13} = -K_{wr}a_2, K_{19,19} = K_{wr};$

In which, C_s and K_s are the damping coefficient and stiffness of spring of driver seat; C_c and K_c are the damping and stiffness of each spring of cab suspension; C_1,C_2 are front suspension damping; $C_{3\sim6}$ are the drive suspension coefficient; C_e is the effective damping coefficient of drive axle suspension; K_f is the stiffness of each spring of front axle suspension; K_m, and K_r are defined for stiffness of every spring for the middle axle and the rear axle, respectively; K_{wf} is also considered for the equivalent stiffness of each of front tires, while K_{wr} plays the same role for the tires of middle and rear wheels. Other variables and constants were illustrated in the previous sections.

The developed dynamic model is 19 DoF, which includes the truck and its 6 wheels. However, in trucks motion analysis under sinusoidal road surface excitation, because of that the truck is placed on the road and the effect of the excitations of the road surface on the motions of the 6 wheels, therefore a 13 DoF system have been used as a simplified model of the 19 DoF model stiffness matrix and the proper model.

The following sinusoid inputs is the excitations profile of the road surface that applies to the wheels:

$w_i = A_r \sin(\omega_{dr} t + \phi_i);$
$1,2,\dots,6$
(6)

$$\omega_{dr} = 2\pi\left(\frac{v}{L}\right); \qquad (7)$$

Where A_r is road roughness magnitude in meter, ω_{dr} is drive frequency in rad/s, v is truck forward speed in m/s, L is Road surface wave length in meter and ϕ_i is the phase angle of the nth wheel in rad.

And the equation of motion is as below:

$$M.\ddot{W} + C.\dot{W} + K.W = f(t); \qquad (8)$$

Where $\mathbf{M}$ is system mass matrix, $\mathbf{C}$ is damping matrix, $\mathbf{K}$ is stiffness matrix, $\ddot{W}$ is acceleration vector, $\dot{W}$ is velocity vector, W is displacement vector, all of the 13 DoF truck model and $f(t)$ is road excitation vector, which is defined in the form of:

$$f(t) = \begin{bmatrix} 0 \\ \vdots \\ 0 \\ k_{w1}A_r\sin(\omega_{dr}t+\phi_1) + k_{w2}A_r\sin(\omega_{dr}t+\phi_2) \\ k_{w1}a_2A_r\sin(\omega_{dr}t+\phi_1) - k_{w2}a_2A_r\sin(\omega_{dr}t+\phi_2) \\ k_{w3}A_r\sin(\omega_{dr}t+\phi_3) + k_{w4}A_r\sin(\omega_{dr}t+\phi_4) \\ k_{w3}a_2A_r\sin(\omega_{dr}t+\phi_3) - k_{w4}a_2A_r\sin(\omega_{dr}t+\phi_4) \\ k_{w5}A_r\sin(\omega_{dr}t+\phi_5) + k_{w6}A_r\sin(\omega_{dr}t+\phi_6) \\ k_{w5}a_2A_r\sin(\omega_{dr}t+\phi_5) - k_{w6}a_2A_r\sin(\omega_{dr}t+\phi_6) \end{bmatrix}_{(13\times1)}$$

As mentioned system matrices in Equation (8) is 13×13, the vector G (gravity vector) does not appear here, because the systems initial positions are chosen to be in the equilibrium positions.

Central difference method has been utilized for numerical solution and dynamic simulation, the well-known equation for it is as below:

$$\ddot{w} \approx \frac{W_{t+\Delta t} - 2w_t + w_{t-\Delta t}}{(\Delta t)^2}; \qquad (9)$$

$$\dot{w} \approx \frac{w_{t+\Delta t} - w_{t-\Delta t}}{2\Delta t}; \qquad (10)$$

The continuous sinusoidal variation of the road profile, which is used in the simulation, is as below:

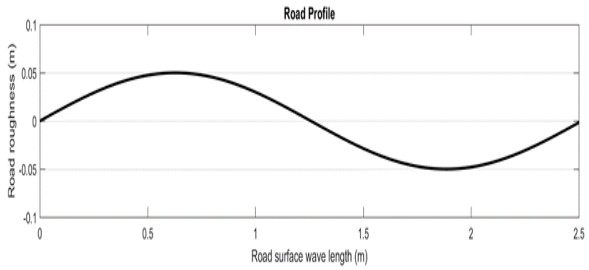

Fugure 5. Road profile

In this paper, for simulating typical road conditions, two drive frequencies have been used. The low drive frequency is chosen to have a magnitude of 2 Hz and the higher drive frequency have a magnitude of 12 Hz. The difference between the road roughness excitations caused by these two drive frequencies is showed in figure below:

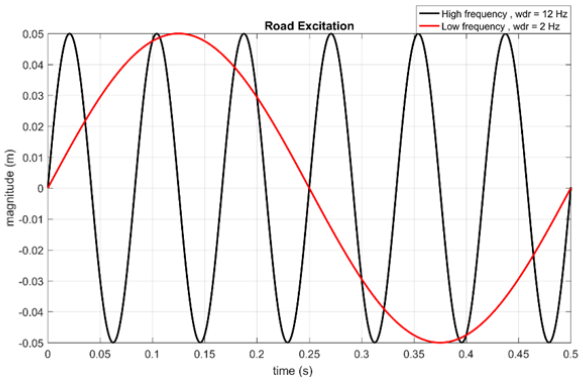

Figure 6. The high and low frequency for road excitations cases.

Two cases have been chosen for phase angle (ϕ). In one case the right steer wheel and the left steer wheel have no phase difference, and this means that ϕ12 is equal to 0 and in the other case we have considered 90 degrees' phase lag for the right steer wheel compared to the left steer wheel and this similarly means that ϕ12 is equal to π/2. For comparison, these two cases with various phase angles are showed in Figure 7.

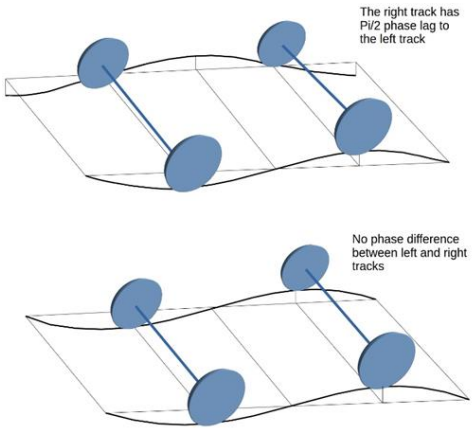

Figure 7. various excitation phase angles between the right and the left wheel.

By considering the depicted phase angles, the nth wheel's phase angle (ϕn) is evaluated as follow:

$$\phi_1 = 0;$$

$$\phi_2 = \phi_1 - \phi_{12};\ \phi_3 = \phi_1 - \phi_{13};\ \phi_4 = \phi_2 - \phi_{24};$$

$$\phi_5 = \phi_1 - \phi_{15};\ \phi_6 = \phi_2 - \phi_{26};$$

Where ϕ12, ϕ13, … are wheel 1 and 2, wheel 1 and 3, etc. phase angle difference as following:

ϕ_12=0 or π/2 ; (depends on case of study);

$$\phi_{13} = \frac{2\pi(b_1 - b_2)}{L};$$

$$\phi_{15} = \frac{2\pi(b_1 - b_3)}{L};\ \phi_{24} = \phi_{13};\ \phi_{26} = \phi_{15};$$

L is the wave length of road surface in meter and b1, b2, b3 are some geometric distance, depicted in figure 4.

The drive frequency for the truck can be specified in two ways. In one way by assuming a specific road with a fixed wave length of L, a higher drive frequency means that the truck is running in a higher speed, while in a lower drive frequency the truck is running at a lower speed. Analogously for the other way, if we consider a fixed truck speed, a higher drive frequency means that the road surface has short wavelength characteristics, while in a lower drive frequency the road surface has long wavelength characteristics. Therefore, the assumptions in the simulation strongly affects the simulation results. In this paper, the wave length of the road is considered to be fixed and the truck speed is set to either the high and low values of 30m/s and 5m/s, respectively. By considering two different ϕn settings this gives us four cases in total, for case 1 and 2 we have a high drive frequency and for case 3 and 4 we have low dive frequency, for all cases ωdr is 2Hz and Ar is 0.05m, for case 1 and 3, ϕ12 is equal to zero and for case 2 and 4, ϕ12 is equal to π/2. Finally, by programming the equations in MATLAB software, the simulation results are achieved.

3. RESULTS

The results for the four expressed cases are shown by the following figures as system time response for the different cases.

Case 1:

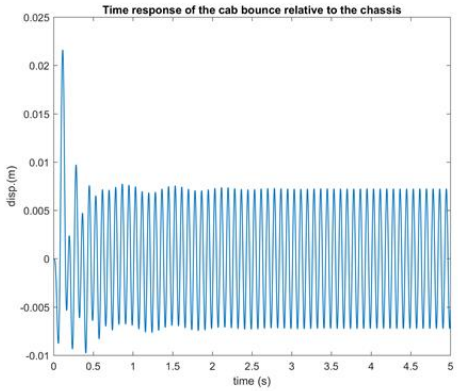

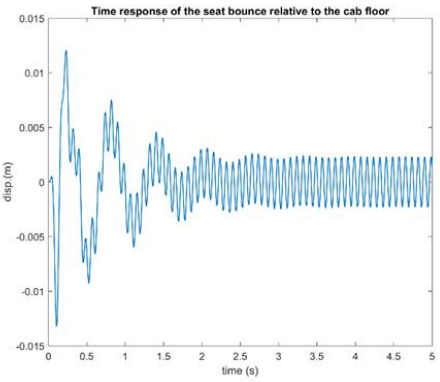

Figure 8. Cab to chassis and seat to cab floor relative bounce time response in high drive frequency for $\phi 12 = 0$

Case 2:

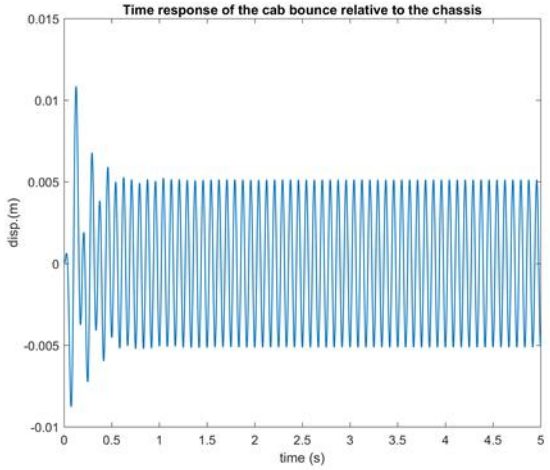

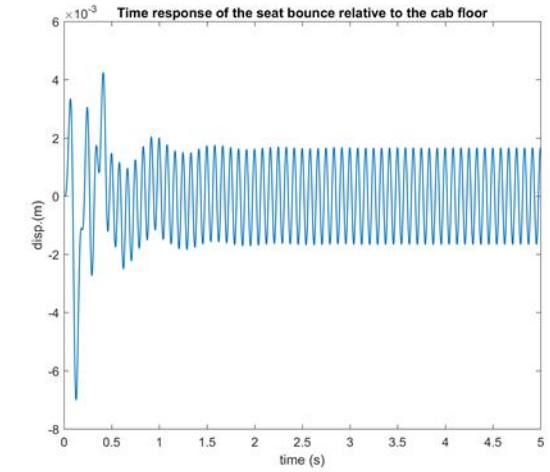

Figure 9. Cab to chassis and seat to cab floor relative bounce time response in high drive frequency for $\phi 12 = \pi/2$.

Case 3:

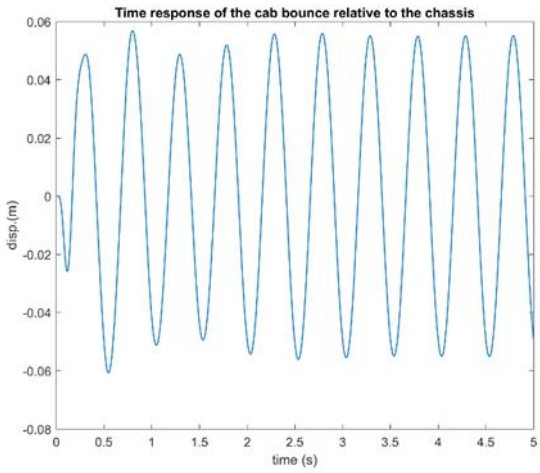

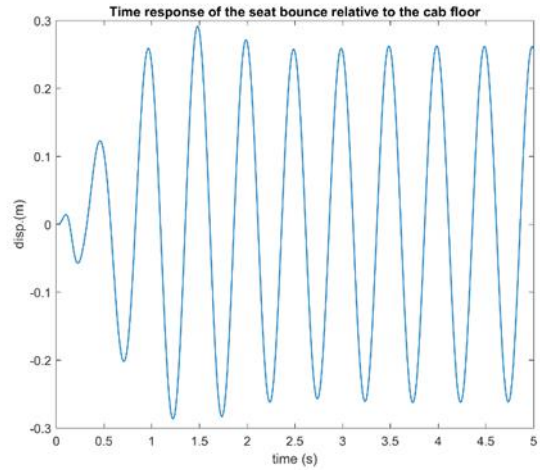

Figure 10. Cab to chassis and seat to cab floor relative bounce time response in low drive frequency for $\phi 12 = 0$

Case 4:

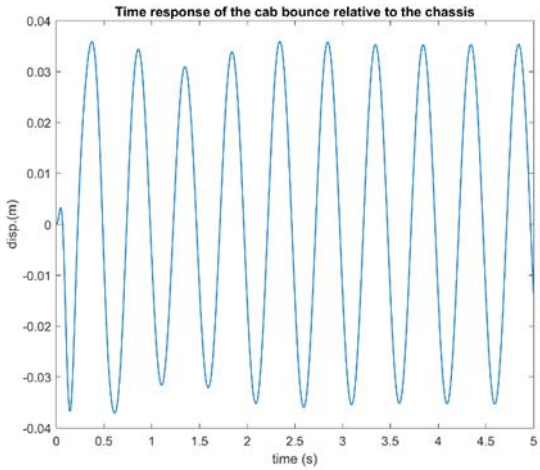

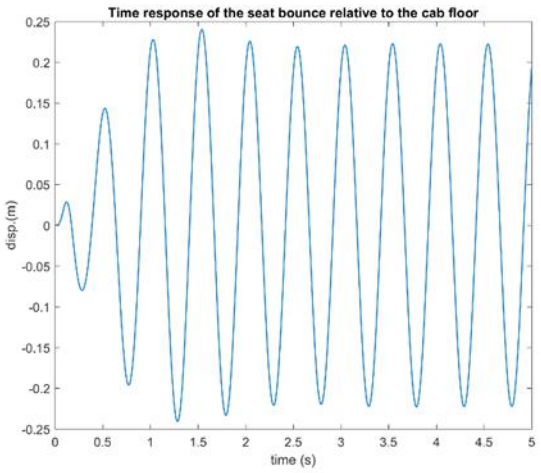

Figure 11. Cab to chassis and seat to cab floor relative bounce time response in low drive frequency for $\phi 12 = \pi/2$

These cases from Figure 8 to Figure 11 shows the bounces of the seat and the cab relative to the cab floor and the chassis, respectively as it is more conventional to measure in this way. Results illustrates that the seat has an acceptable vibration isolation performance in high frequency excitations. However, in relatively lower frequency excitations, it is clear that the vibration level is extremely high and is greatly magnified.

4. CONCLUSION

The three-axle truck in this work have been modeled as a 19-DoF system. The linear model of the truck has some unique features which includes the cab suspension, the seat suspension and the suspension geometry, this features are vital in ride modeling for heavy vehicles but are often ignored. The physical properties of the truck are evaluated by modelling the truck in SOLIDWORKS software. The equations of motion are obtained by using the Lagrange equation. To obtain the system responses subject to sinusoidal road excitations numerical central difference method is assisted. Finally, system's time responses have been gained under four cases for the truck in low and high speed motions, these are useful to know the vibrating component of the truck. Although, some of these results may only affect this special truck model, they will help to better understand the traits of this kind of vehicles and also will help to understand how to develop more realistic nonlinear models.

5. REFERENCES

[1] Ali Rahmani, Ali Mirmohammadi, S. M. Javad Zeidi, Saeed Shojaei, "Numerical Approach toward Calculation of vibration Characteristics of the Multi Axles Truck Using Lagrange Method".

[2] Saeed Shojaei, S. M. Javad Zeidi, Ali Rahmani, Ali Mirmohammadi, "Analytical Analysis Approach to Study of the Vibration Characteristics of the Multi Axles Truck and its Validation".

[3] Hamedi, A., Ketabdar, M. (2016). Energy Loss Estimation and Flow Simulation in the skimming flow Regime of Stepped Spillways with Inclined Steps and End Sill: A Numerical Model. International Journal of Science and Engineering Applications, 5(7), 399-407.

[4] Kadkhodapour, J. and S. Raeisi, Micro–macro investigation of deformation and failure in closed-cell aluminum foams. Computational Materials Science, 2014. 83: p. 137-148.

[5] Ketabdar, M. Hamedi, A. (2016). Intake Angle Optimization in 90-degree Converged Bends in the Presence of Floating Wooden Debris: Experimental Development. Florida Civil Engineering Journal, 2, 22-27.

[6] Sheikholeslami ,A. and L. Azizi, (2010). Safety Analysis of Constructed U-turns in the City of Tehran], Journal of Transportation Research 7 (223), 167-184.

[7] Azizi, L. and A. Sheikholeslami, (2013). Safety effect of U-turn Conversions in Tehran: Empirical Bayes Observational Before and After Study and Crash Prediction Models", Journal of Transportation Engineering 139 (1),101-108.

[8] Kadkhodapour, J., H. Montazerian, and S. Raeisi, Investigating internal architecture effect in plastic deformation and failure for TPMS-based scaffolds using simulation methods and experimental procedure. Materials Science and Engineering: C, 2014. 43: p. 587-597.

[9] Sheikholeslami, A and L. Azizi, (2010) Observational Before-After Study of the Safety Effect of U-turns Conversions Using the Empirical Bayes Method, 15th International Conference on Road Safety CMRSC-XX

[10] Mardanpour, P., Izadpanahi, E., Rastkar, S., Fazelzadeh, S. A., & Hodges, D. H. (2017). Geometrically Exact, Fully Intrinsic Analysis of Pre-Twisted Beams Under Distributed Follower Forces. AIAA Journal, 1-13.

[11] Mardanpour, P., Izadpanahi, E., Rastkar, S., & Hodges, D. H. (2017). Nonlinear Aeroelastic Gust Suppression and Engine Placement. Journal of Aircraft, 1-4.

[12] Mardanpour, P., Izadpanahi, E., Rastkar, S., & Hodges, D. H. (2017). Effects of engine placement on nonlinear aeroelastic gust response of high-aspect-ratio wings. In AIAA Modeling and Simulation Technologies Conference (p. 0576).

[13] Watts GR (1987) Traffic-induced ground-borne vibrations in dwellings. Research Report 102, Transport and Road Research Laboratory, Crowthorne, Berkshire

[14] Hunt HEM (1991) Modelling of road vehicles for calculation of traffic-induced ground vibrations as a random process. J Sound Vib 144(1):41–51. doi:10.1016/0022-460X(91)90731-X

[15] Cebon D (1993) Interaction between heavy vehicles and roads. Warrendale (USA): Society of Automotive Engineers, SP 951: ISBN: 1-56091-336-3

[16] Mamlouk MS (1997) General outlook of pavement and vehicle dynamics. J Transport Eng 123(6): 515-517. ISSN: 0733-947X

[17] Liu C, Herman R (1998) Road profiles, vehicle dynamics, and human judgement of serviceability of roads: spectral frequency domain analysis. J Transport Eng 124(2):106–111. doi:10.1061/(ASCE)0733-947X(1998)124:2(106)

[18] Melcer J (2006) Vehicle-road interaction, analysis in a frequency domain. Slovak J Civil Eng 3: 48–52. ISSN: 1210-3896

[19] Dodds CJ, Robson JD (1973) The description of road surface roughness. J Sound Vib 31(2):175–183. doi:10.1016/S0022-460X(73)80373-6

[20] Rahmani, F., Razaghian, F. and Kashaninia, A.R., 2015. Novel Approach to Design of a Class-EJ Power Amplifier Using High Power Technology. World Academy of Science, Engineering and Technology, International Journal of Electrical, Computer, Energetic, Electronic and Communication Engineering, 9(6), pp.541-546.

[21] Wambold JC, Defrain LE, Hegmon RR, Macghee K, Reichert J, Spangler EB (1981) State of the art of measurement and analysis of road roughness. Transport Res Rec 836: 21–29. ISSN: 0361-1981

[22] ISO 8608 (1995) Mechanical vibration, road surface profiles. Reporting of Measured Data

[23] Andren P (2006) Power spectral density approximations of longitudinal road profiles. Int J Veh Des 40(1/2/3):2–14. doi:10.1504/IJVD.2006.008450

[24] Elson MJ, Bennet JM (1995) Calculation of the power spectral density from surface profile data. Appl Opt 34:201–208. doi:10.1364/AO.34.000201

[25] Feng T, Yu-Fen H, Shun-Hsu T, Wes SJ (2006) Generation of random road profiles. CSME: B04-001: 1373-1377

[26] Azizi, L., MS. Iqbal and M.Hadi,(2018), Estimation of Freeway Platooning Measures Using Surrogate Measures Based on Connected Vehicle Data, Presented at 97st Annual Meeting of Transportation Research Board, Washington DC.

[27] Wong. J, Y.," Theory of ground vehicles". John Wiley & Sons, Canada. (2001)

[28] Rahmani, F., Razaghian, F. and Kashaninia, A.A., 2014. High Power Two-Stage Class-AB/J Power Amplifier with High Gain and Efficiency. Journal of Academic and Applied Studies (JAAS), 4(6), pp.56-68.

[29] Jazar, R., "Advanced Vibrations:A modern Approach", Springer, New York. (2013).

[30] Jazar, R., "Vehicle Dynamics: Theory and Application", Springer, New York. (2010).

[31] Gillespie, T, D., "Fundamentals of Vehicle Dynamics", SAE publishing group, United States of America. (1992).

[32] Yang, X., Zengcai, W., Weili, P., "Coordinated Control of AFS and DYC for Vehicle Handling and Stability Based on Optimal Guaranteed Cost Theory," Vehicle System Dynamics, 47, pp. 57-79 (2009).

[33] Zheng, S., Tang, H., Han, Z., Zhang, Y., "Controller Design for Vehicle Stability Enhancement," Control Engineering Practice, 14, pp. 1413-1421 (2006).

[34] A. Rahmani-Hanzaki, S. K. Saha, and P. V. M. Rao, An improved recursive dynamic modeling of a multibody system with spherical joint, Int, J, of Multibody system dynamics, 21, pp. 325-345, (2009).

[35] Tabatabaee, S,H,. "Integrated control to improve directional stability and maneuverability of the articulated heavy vehicle", PhD Thesis, K. N. Toosi University of Technology Faculty of Mechanical Engineering, (2013).

[36] Zeidi, SMJ, Hoseini, P., Rahmani, A., (2017). Study of vibration specifications of a three-axle truck using Lagrange method, Journal of Modern Processes in Manufacturing and Production, vol. 6(1), pp. 83-95.

[37] Zeidi, SMJ, Hoseini, P., Rahmani, A., (2017). Modeling a Three-axle Truck and Vibration Analysis under Sinusoidal Road Surface Excitation, International Journal of Science and Engineering Applications Volume 6 Issue 09, 2017.

[38] Zeidi, SMJ and Mahdi, M. 2015. Investigation effects of injection pressure and compressibility and nozzle entry in Diesel injector nozzle's flow. Journal of Applied and Computational Mechanics. 1(2):83–94.

[39] Zeidi, SMJ., and Mahdi, M. 2015. Effects of nozzle geometry and fuel characteristics on cavitation phenomena in injection nozzles. Proceedings of the 22st Annual International Conference on Mechanical Engineering-ISME.

[40] Zeidi, SMJ. and Mahdi. M. 2014. Investigation of viscosity effect on velocity profile and cavitation formation in Diesel injector nozzle. Proceedings of the 8th International Conference on Internal Combustion Engines.

[41] Zeidi, SMJ. and Mahdi, M. 2015. Evaluation of the physical forces exerted on a spherical bubble inside the nozzle in a cavitating flow with an Eulerian/Lagrangian approach, European Journal of Physics, 36(6):41-65.

[42] SM Aghaei, MM Monshi, I Torres, SMJ Zeidi, I Calizo, 2018, DFT study of adsorption behavior of NO, CO, NO2, and NH3 molecules on graphene-like BC3: A search for highly sensitive molecular sensor, Journal of Applied Surface Science, 427, PP. 326-333.